Nonphotochemical hole-burning studies of energy transfer dynamics in antenna complexes of photosynthetic bacteria

by

Satoshi Matsuzaki

A thesis submitted to the graduate faculty

in partial fulfillment of the requirements for the degree of

MASTER OF SCIENCE

Major: Physical Chemistry

Major Professor: Gerald J. Small

Iowa State University

Ames, Iowa

2001

ACKNOWLEDGMENTS

I would like to take this opportunity to express my genuine thanks to those who assisted me during of my thesis research.

I am indebted to my research advisor, Professor Gerald Small, for his guidance, patience and numerous discussions in the past few years. I am fortunate to benefit from his knowledge and insights in various subjects.

Dr. Valter Zazubovich and Dr. Margus Rätsep deserve my sincere appreciation and much credit for the work presented in this thesis. I would like to acknowledge Dr. John Hayes for providing invaluable advices. I am also particularly grateful to Dr. Tõnu Reinot for his various suggestions to this thesis work and providing me some great figures. I am also grateful to Dr. Ryszard Jankowiak for his assistance and expertise.

I am particularly thankful to Dr. Kenneth Roberts for helpful discussions and (soon to be Dr.) Richard Walsh who spent hours proofreading my writing.

Most of all, my sincere thank goes to Ms. Tiffany Fraser for her continuous support and understanding that kept me focused on completing my thesis studies.

This work was performed at Ames Laboratory under Contract No. W-7405-Eng-82 with the U.S. Department of Energy. The United States government has assigned the DOE Report number IS-T 2110 to this thesis.

APPENDIX. 2-MODE/3-GAUSSIAN HOLE PROFILE SIMULATION PROGRAM

Following is the program used to test to fit the experimental hole spectra of FMO complex described in Chapter 3. The original program (1-Gaussian) was written by Dr. John Hayes in C/C++ to calculate hole profiles analytically in the short burn time limit, according to our groups' hole burning theory [1,2]. Variety of hole profile simulation programs have been written and revised by former members of our group, including Dr. Inja-Lee, Dr. Luchuan Shu, Dr. Paul Lyle and by Dr. John Hayes [2,3].

My contribution to the program was the conversion of the program into Wolframs' *Mathematica*® script language (see Refs. [4-6] for details on formats and functions), which allows user to use actual integration for the absorption spectrum calculation rather than using approximation by Bode function. The program below (in cell-expression format) was written in compatible with *Mathematica* 2.2x and 3.0 and it was tested under 32bits Microsoft Windows version of '*Mathematica* for Students version 3.0'. Descriptions of calculation variables and other information are included in the program itself. Combining the 2-mode profiles generated the 5-mode single-site absorption profile presented in Chapter 1.

One of the possible future works would be the incorporation of tunneling parameter (Gaussian distribution) into the hole-burning quantum yield variable, ϕ, as discussed in recently published papers [7,8]. Also, revisions and algorithm changes may be necessary for faster calculation.

CHAPTER 1. GENERAL INTRODUCTION TO BACTERIAL ANTENNA COMPLEXES

1.1 Thesis Organization

This thesis contains the candidate's original work on excitonic structure and energy transfer dynamics of two bacterial antenna complexes as studied using spectral hole-burning spectroscopy. The general introduction is divided into two chapters (1. and 2.). Chapter 1 provides background material on photosynthesis and bacterial antenna complexes with emphasis on the two bacterial antenna systems related to the thesis research. Chapter 2 reviews the underlying principles and mechanism of persistent nonphotochemical hole-burning (NPHB) spectroscopy. Relevant energy transfer theories are also discussed. Chapters 3 and 4 are papers by the candidate that have been published. Chapter 3 describes the application of NPHB spectroscopy to the Fenna-Matthews-Olson (FMO) complex from the green sulfur bacterium *Prosthecochloris aestuarii*; emphasis is on determination of the low energy vibrational structure that is important for understanding the energy transfer process associated within three lowest energy Q_y-states of the complex. The results are compared with those obtained earlier on the FMO complex from *Chlorobium tepidum*. In Chapter 4, the energy transfer dynamics of the B800 molecules of intact LH2 and B800-deficient LH2 complexes of the purple bacterium *Rhodopseudomonas acidophila* are compared. New insights on the additional decay channel of the B800 ring of bacteriochlorophyll *a* (BChl *a*) molecules are provided. General conclusions are given in Chapter 5. A version of the hole spectrum simulation program written by the candidate for the FMO complex study (Chapter 3) is

CHAPTER 2. GENERAL INTRODUCTION TO NONPHOTOCHEMICAL HOLE-BURNING SPECTROSCOPY

2.1 General Introduction to Hole-burning Spectroscopy

Fundamental mechanisms and applications of hole-burning spectroscopy and theories related to hole spectra are covered in this chapter. These theories are the foundation for simulations of hole spectra for the FMO complex study (Chapter 3). In addition, molecular exciton theory is briefly described to provide background on the exciton level structure calculations reported in the study of the LH2 complex (Chapter 4).

The optical absorption bands of chromophores in amorphous solid hosts such as glasses and polymers exhibit large inhomogeneous broadening. This is also the case for Chls in proteins. Such broadening is the result of a chromophore experiencing different environments, i.e. interactions between the chromophore and the host molecules gives rise to a distribution of transition frequencies [1]. A schematic illustration of this is depicted in the Figure 2.1. Typical inhomogeneous broadening of electronic absorption bands are Γ_{inh} ~100–300 cm^{-1} [2]. On the other hand, each particular chromophore carries a finite width, which is called homogeneous width (γ) and is determined by the total dephasing time (T_2) associated with the optical transition of the chromophore in its environment. The linewidth of the homogeneous broadening is given by

$$\gamma(\mathrm{cm}^{-1}) = \frac{1}{\pi T_2 c}, \tag{1}$$

where T_2, the total dephasing time, is defined [3] by

Figure Captions

Figure 1. The 4.2 K Q_y-absorption spectrum of the FMO complex from *P. aestuarii* (solid curve) and *Cb. tepidum* (dashed curve).

Figure 2. Hole burned spectra of the FMO complex from *P. aestuarii* obtained with burn wavelength (λ_B) = 823.0 nm at 4.2 K. For convenience the absorption spectrum is also shown. From top to bottom the burn intensity and burn time used were: 50 mW/cm^2, 30 s; 100 mW/cm^2, 75 s; and 100 mW/cm^2, 375 s. The deepest and sharpest hole in each spectrum is the resonant zero-phonon hole at λ_B = 823.0 nm. The solid arrows locate the 18 cm^{-1} pseudo-phonon sideband hole (PSBH). The satellite holes a, b and c correspond to those indicated in Figures 4 and 5. The broad and higher energy holes are the result of the structural changes that accompany hole burning in the 825 nm absorption band. The structural changes alter the energies of the states that contribute to the higher energy absorption band, see text.

Figure 3. Spectra of the FMO complex from *P. aestuarii* related to the white light hole burning effect, cf. text for discussion. For convenience the absorption spectrum is also shown. The excessive noise in the spectra near 815 nm is due to the high absorbance. T = 4.2 K.

Figure 4. The dependence of the 4.2 K hole burned spectrum of the FMO complex from *P. aestuarii* on burn wavelength (818.0 – 829.3 nm). The deepest hole in each spectrum is the resonant zero-phonon hole located at λ_B. The burn intensities and times used to obtain the λ_B = 818 – 824 nm spectra were 100 mW/cm^2 and 375 s. The intensity and time for the λ_B = 824.7 and 829.3 nm were 125 mW/180 s and 250 mW/660 s, respectively. The solid arrows locate the 18 cm^{-1} pseudo-PSBH; the dashed arrow in the λ_B = 829.3 nm locates the real-PSBH due to the 18 cm^{-1} phonon. The energies of holes a – f as measured relative to λ_B are given in Table 1. The dashed curve is the

CHAPTER 3. ENERGY TRANSFER KINETICS AND LOW ENERGY VIBRATIONAL STRUCTURE OF THE THREE LOWEST ENERGY Q_Y-STATES OF THE FENNA-MATTHEWS-OLSON ANTENNA COMPLEX

A paper published in the *Journal of Physical Chemistry B* **2000**, 104, 9564.

S. Matsuzaki, V. Zazubovich, M. Rätsep, J. M. Hayes, and G. J. Small

Abstract

Burn wavelength (λ_B)-dependent nonphotochemical hole spectra are reported for the lowest energy Q_y-absorption band of the Fenna-Matthews-Olson (FMO) trimer complex from *Prosthecochloris aestuarii*. This band at 825 nm is contributed to by three states that stem from the lowest energy state of the subunit of the trimer. The spectra reveal unusually rich and quite sharp low energy satellite structure that consists of holes at 18, 24, 36, 48, 72, 120 and 165 cm^{-1} as measured relative to the resonant hole at λ_B. The possibility that some of these holes are due to correlated downward energy transfer from the two higher energy states that contribute to the 825 nm band could be rejected. Thus, the FMO complex is yet another example of a photosynthetic complex for which structural heterogeneity results in distributions for the values of the energy gaps between Q_y-states. The results of theoretical simulations of the hole spectra are consistent with the above holes being due to intermolecular phonons and low energy intramolecular vibrations of the bacteriochlorophyll *a* (BChl *a*) molecule. The 36 cm^{-1} and higher energy modes are most likely due to the intramolecular BChl *a* modes. The simulations lead to the determination of the Huang-Rhys (S) factor for all modes. They range

Figure Captions

Figure 1. The 4.2 K absorption spectra of intact (a) and B800-deficient LH2 (b) normalized to equal peak intensities of the B850 band. Inset: spectrum (b) is an expanded view of the 800 nm region of B800-deficient LH2; spectrum (c) is that of the same sample after storage in the dark at 0°C for one week.

Figure 2. Widths of zero-phonon holes burned into the B800 band with different burn frequencies at 4.2 K (inset). The burn intensity and time were ~ 120 mW/cm^2 and 100 s. The fractional hole depths were 0.02–0.03. The uncertainty in the widths is ± 0.3 cm^{-1}. Thus, the holewidth is independent of burn frequency. The average of the holewidths is 3.2 ± 0.3 cm^{-1} which corresponds to a B800? B850 transfer time of 3.2 ps (see text for discussion). For convenience the absorption spectrum from Figure 1 is shown.

Figure 3. Widths of zero-phonon holes burned into the B800 band of intact LH2. The diamond data points are from this study. The burn intensity and time were ~ 120 mW/cm^2 and 100 ps. Fractional hole depths did not exceed 0.03. The solid circle data point is from Ref. [16] and corresponds to a holewidth of 26 cm^{-1}. Importantly, it falls on the straight line defined by the four diamond data points. The inset shows the SDF of the B800 molecules (width = 120 cm^{-1}) and a sigmoidal curve calculated with Eq. 1 with $D(\omega_B-\omega)$ a constant. See text for discussion.

Figure 4. Exciton levels of the B850 ring calculated with the Hamiltonian defined by Eqs. 2–4. The values used for $e_u - e_l$, V_l, V_u and U_{ul} are, respectively (in the unit of cm^{-1}): (a) 600, –200, 100, 130; (b) 600, –270, 170, 200; and (c) 690, –200, 100, 130. The solid and dashed vertical lines denote exciton levels mainly associated with the l- and u-manifolds (see text). The asterisk indicates closely spaced levels of E_2 and E_4 symmetry belonging to the l- an

CHAPTER 4. ENERGY TRANSFER DYNAMICS IN LH2 COMPLEXES OF *RHODOPSEUDOMONAS ACIDOPHILA* CONTAINING ONLY ONE B800 MOLECULE

A paper published in the *Journal of Physical Chemistry B* **2001**, 105, 7049.

S. Matsuzaki, V. Zazubovich, N. J. Fraser, R. J. Cogdell, and G. J. Small

Abstract

Nonphotochemical hole burning (NPHB) and femtosecond pump-probe experiments have previously shown that following their excitation, the B800 molecules of the LH2 complex of *Rhodobacter sphaeroides* and *Rhodopseudomonas* (*Rps.*) *acidophila* relax by two channels. The decay channel observed for excitation on the low energy side of the B800 absorption band is due to B800? B850 excitation energy transfer which occurs in ~ 2 ps at 4 K. The additional decay channel becomes detectable for excitation on the high energy side of the B800 band. The mechanisms that have been proposed for this channel are: (i) vibrational relaxation following excitation of vibronic levels associated with the Q_y-states of either the B800 or B850 bacteriochlorophyll *a* molecules; (ii) direct excitation of upper B850 exciton levels, followed by downward relaxation within the B850 manifold; (iii) intraband B800−B800 energy transfer involving only the B800 molecules; and (iv) downward energy transfer of initially excited mixed B800−B850 states. Presented here are NPHB results for intact LH2 and B800-deficient LH2 complexes of *Rps. acidophila* (strain 10050). The latter contain only one B800 molecule, rather than nine. In sharp contrast with the intact LH2 complex, the zero-phonon holewidths for B800-deficient LH2 complex were observed to be

CHAPTER 5. GENERAL CONCLUSIONS

Nonphotochemical hole-burning (NPHB) spectroscopy was used in this work to study bacterial antenna complexes. The research focused on the Q_y-state electronic structures and energy transfer dynamics of these systems. Theoretical models were used to simulate the data obtained and determine how well the assumptions made in the models successfully describe the systems.

The lowest energy absorption band at 825 nm of FMO complex from *P. aestuarii*, which consists of three states, was burned nonphotochemically and its low energy satellite holes were analyzed to determine the excitation energy transfer (EET) kinetics for the contribution of two higher energy states to the 825 nm band. The satellite holes at 36, 48, 72, 120 and 165 cm^{-1} were concluded, based on simulations, to be pseudo-phonon sideband holes (PSBH) and these phonons were considered due to BChl *a* intramolecular modes. In addition, the temperature dependencies of zero-phonon hole (ZPH) widths burned in the 825 nm band at λ_B = 822.6, 824.6 and 826.6 nm showed similarity to those of *Cb. tepidum* and these three wavelengths were close to the absorption maxima of the three states. Additional energy transfer calculations that account the effects of energy disorder into the electron-phonon coupling parameters were suggested for future study.

NPHB on LH2 complexes of *Rps. acidophila* (strain 10050) that contain only one B800 BChl *a* molecule, in contrast with intact LH2, were performed to determine an additional B800 decay channel. ZPH action spectrum of the lowest exciton level (A symmetry) and the temperature dependency of the B850 absorption band found a deficiency of B800 molecules does not affect on the excitonic structure of the B850 ring.

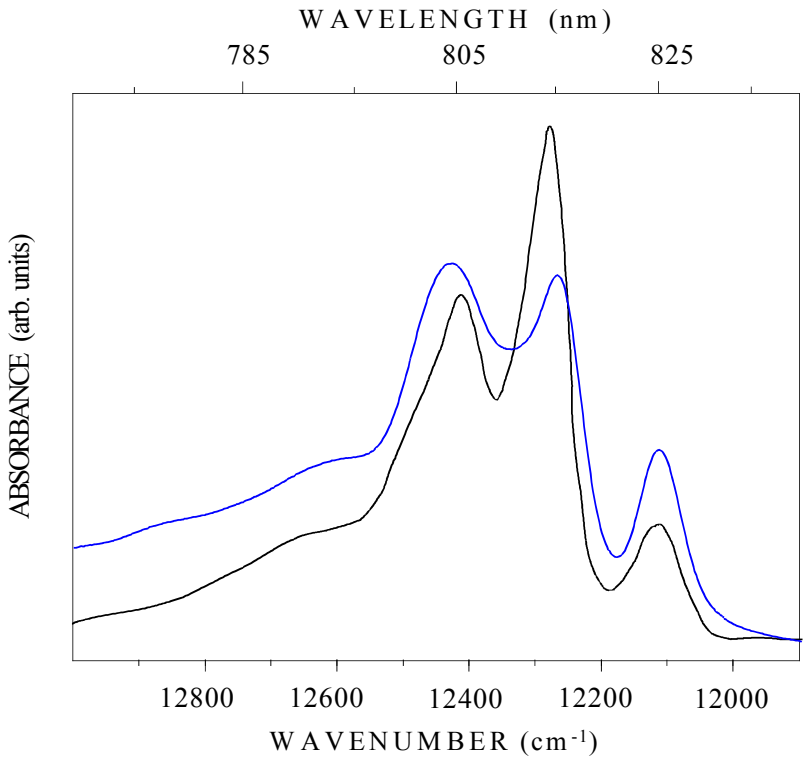

Figure 1.10 The 4.2 K Q_y-absorption spectra of the FMO complexes from *P. aestuarii* (black curve) and *C. tepidum* (blue curve).

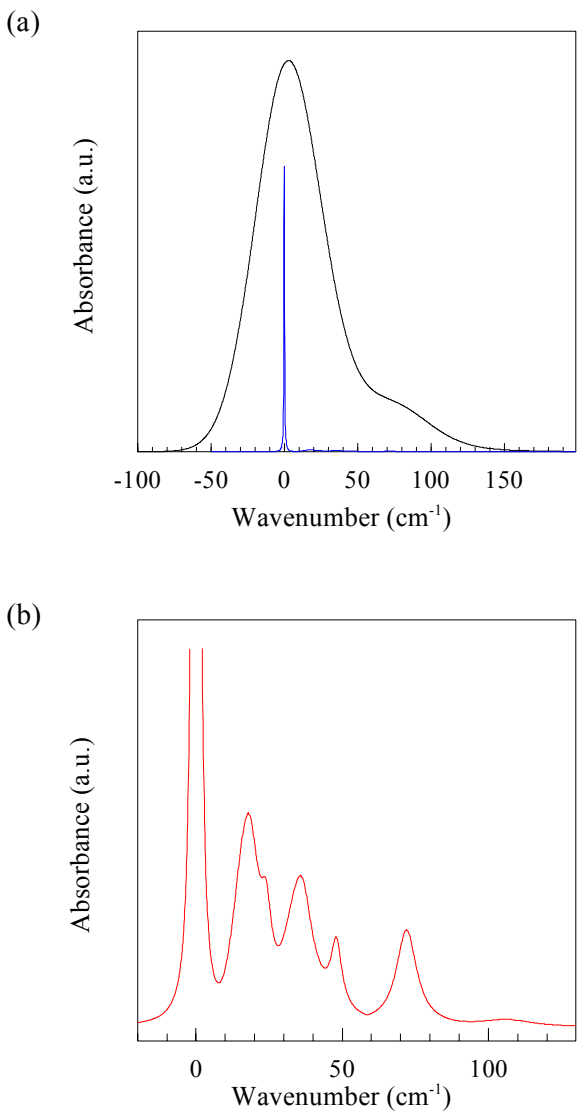

Figure 1.11 Part (a) shows the simulated single-site absorption profile (5-mode) and absorption spectrum, while Part (b) shows a magnified view of the low frequency vibrational sideband structure of the single-site profile for clarification. The simulation parameters used are $\omega\{1..5\}$=18, 24, 36, 48 and 72 cm^{-1} and $S\{1..5\}$=0.24, 0.05, 0.12, 0.04 and 0.12, with bandwidths of 10, 5, 10, 5 and 7.5 cm^{-1}, respectively, as given in Chapter 3. Γ_{inh} = 50 cm^{-1} was used to generate the absorption spectrum.

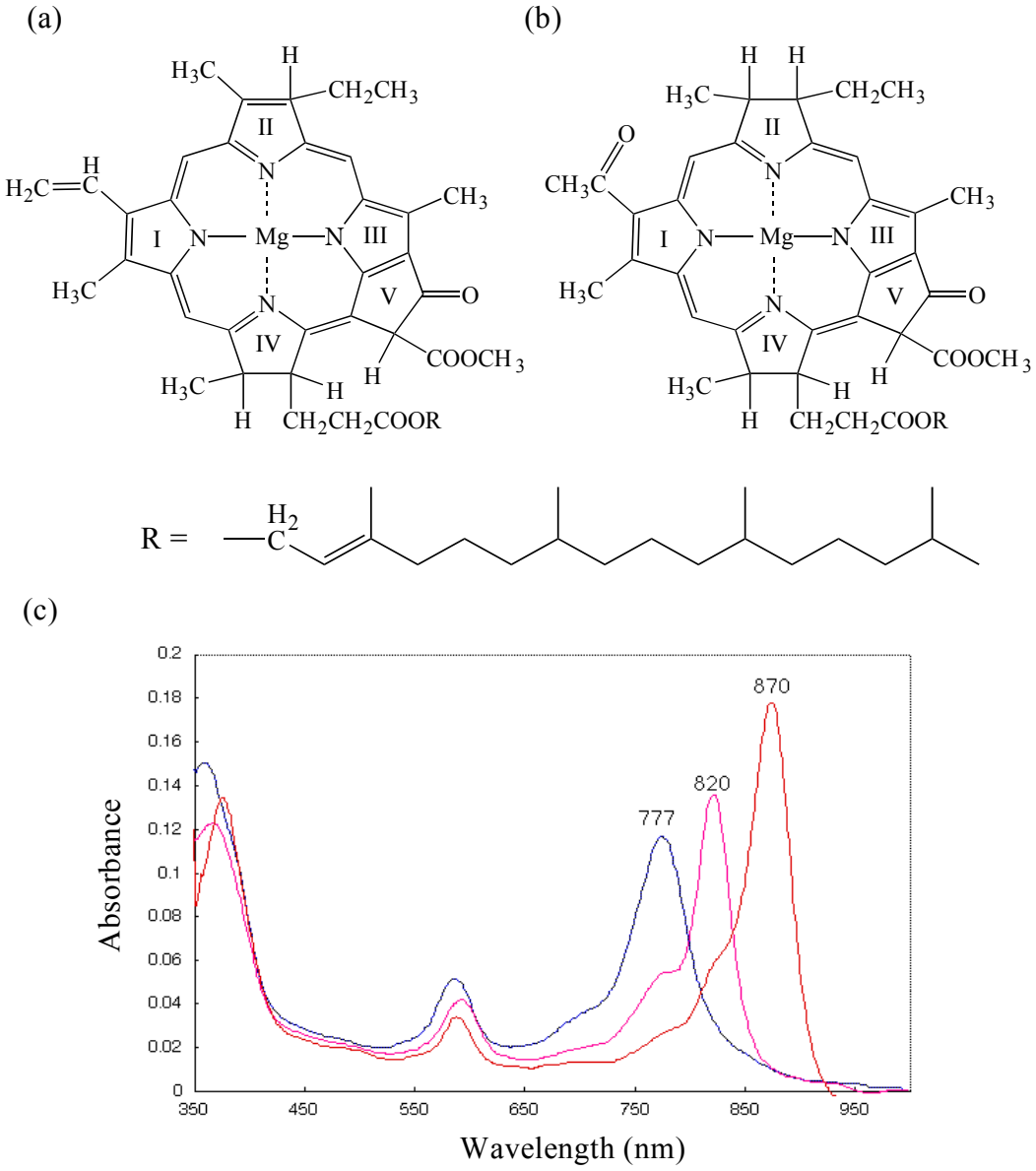

Figure 1.1 Structures of (a) a chlorophyll *a* and (b) a bacteriochlorophyll *a*. The phytyl chain is abbreviated as R in both of the structures. The structures are distinguished, in part, by the saturation/unsaturation in ring II. Part (c) shows room temperature absorption spectra of BChl *a*. The blue spectrum is that of BChl *a* in an organic solvent. The pink and red spectra are those of a dimer and the native LH1 complex that is a cyclic array of 16 BChl *a* dimers, respectively [11].

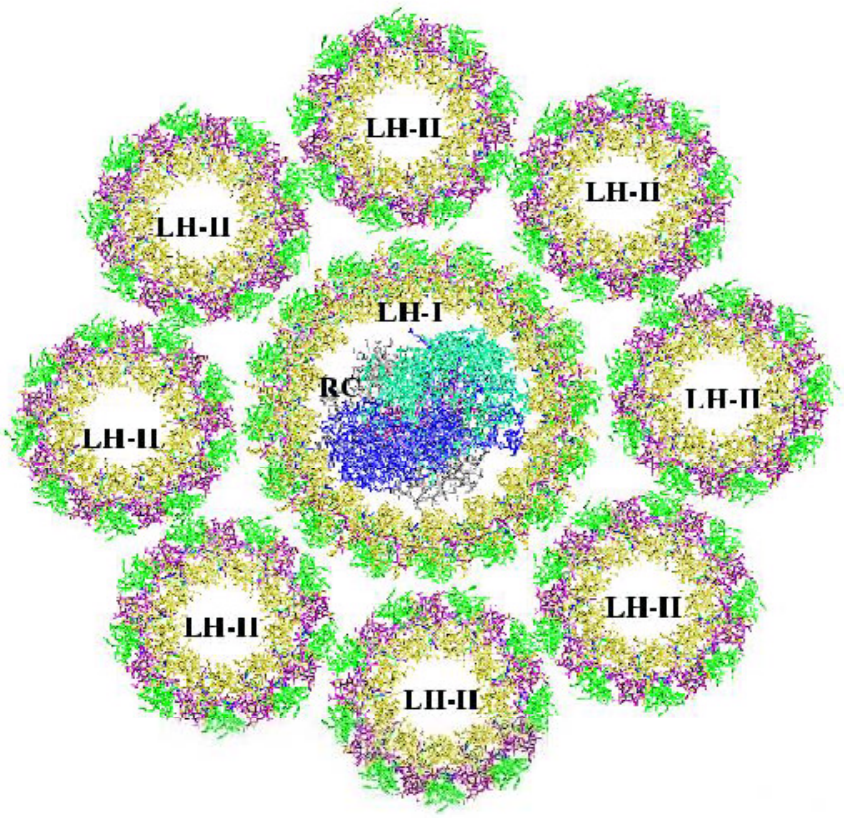

Figure 1.2 Arrangement of light-harvesting complexes in the modeled bacterial photosynthetic unit (PSU) of *Rb. sphaeroides*, in the plane of the special pair of the RC. Original picture was produced with the program VMD [15] and adapted from [16].

(a)

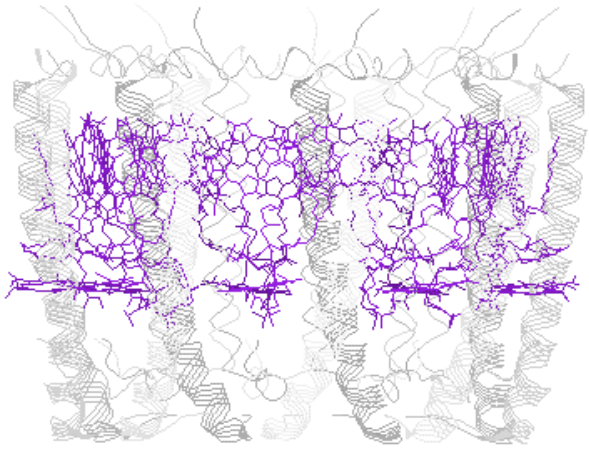

(b)

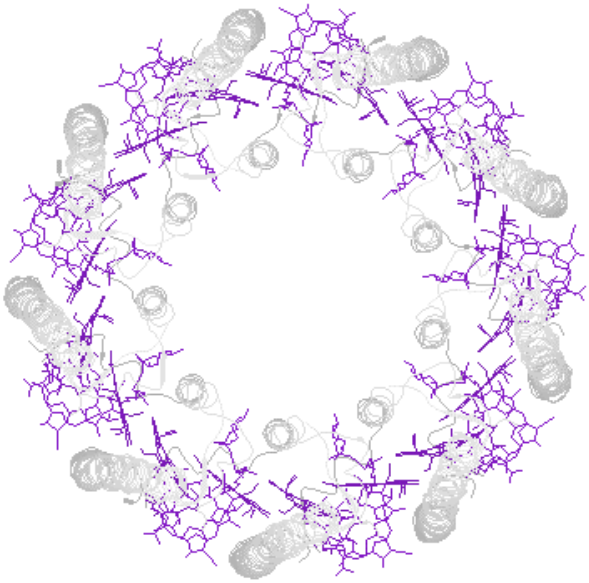

Figure 1.3 Part (a) and (b) show cyclically arranged α–, β–polypeptides of LH2 complex from *Rps. acidophila* (strain 10050) [17,18]. α–polypeptides are located on the inner circle with ~18Å radius, where β–polypeptides are the outer shell having ~34Å radius. BChls are expressed in wireframe forms, where as the rest of the proteins are in strand forms. The figures were

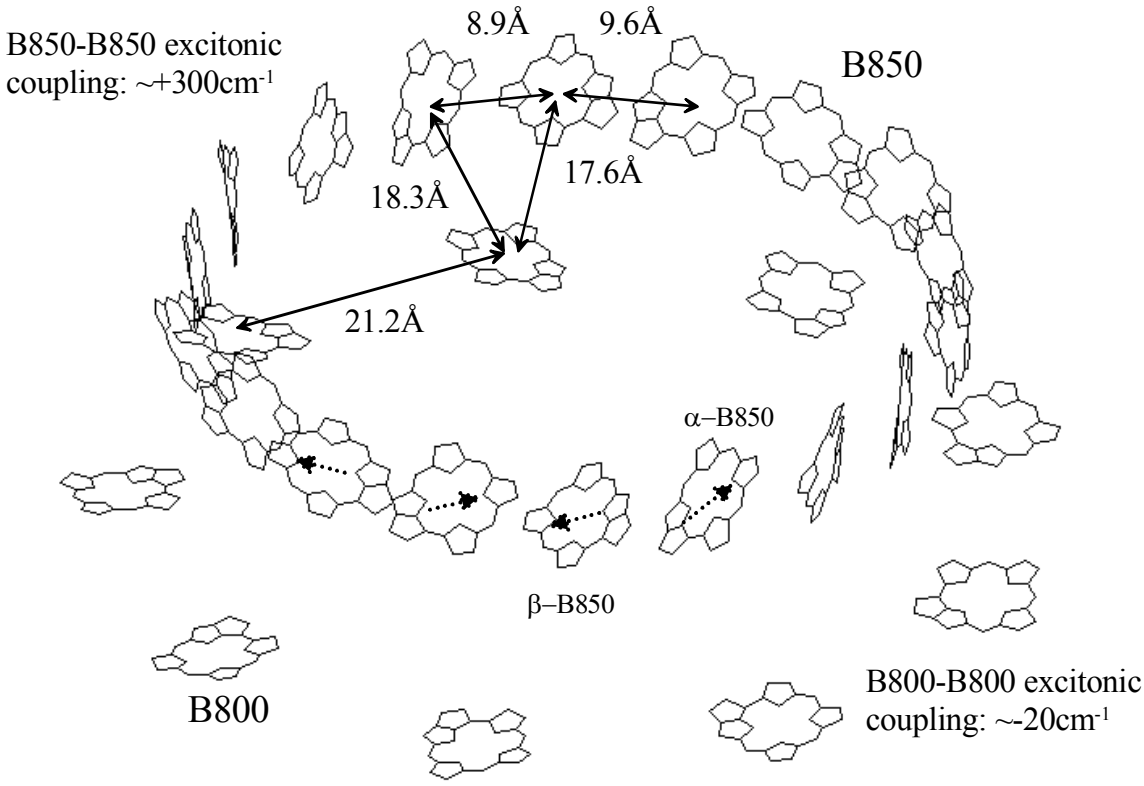

Figure 1.4 Arrangement of the 27 BChls in the LH2 complex from *Rps. acidophila* (strain 10050). All the side chains on the BChls are omitted for clarity. As shown, the upper ring contains 18 B850 molecules, while the lower ring contains nine B800 molecules. Each of the Mg–Mg distances between the BChls is presented with solid arrows. Dotted arrows are also drawn to show the directions of Q_y-transition dipole of the BChls. Excitonic coupling energies between neighboring B800–B800 molecules and between B850–B850

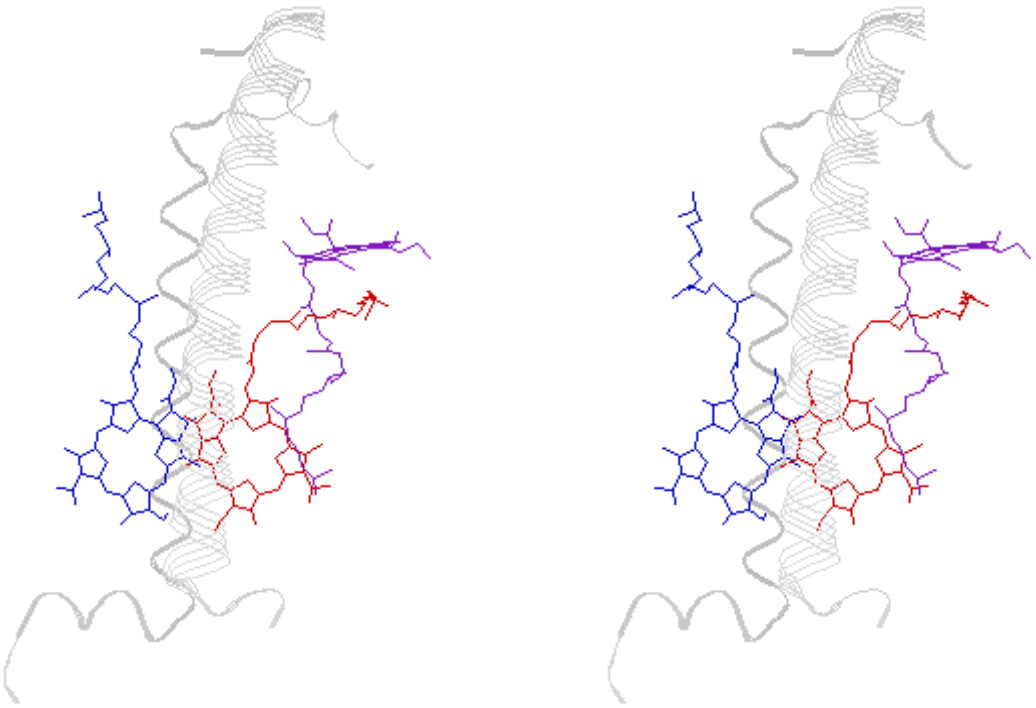

Figure 1.5 Stereographical view of the protomer of the LH2 complex from *Rps. acidophila* (strain 10050), which is the repeating unit of the 9-fold symmetry complex. The front tube represents the α–apoprotein, where as the back ribbon is the β–apoprotein. This figure is a view from the C_9 cylinder center. The BChl *a* molecule that is perpendicular to the C_9 axis is the B800 molecule. Two strongly coupled B850 molecules are located between the α- and β-polypeptides. The α–B850 molecule is in the right

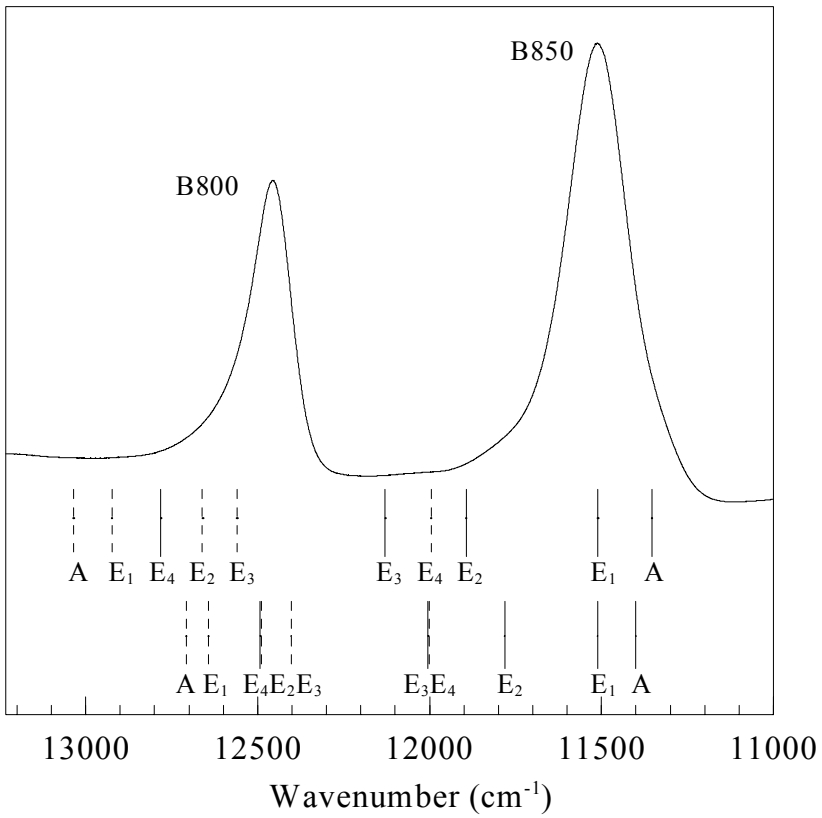

Figure 1.6 Exciton levels of the B850 ring based on simulation with the Hamiltonian defined by Eq. (4). The simulation parameter sets for $e_u - e_l$, V_l, V_u and V_{ul} are 600, –270, 170 and 200 (for upper set – the one presented in Chapter 4) and 600, –200, 100 and 130 (for lower set – given in Sauer et al. [19]), respectively, in the unit of cm^{-1}. The solid and dashed vertical lines represent exciton levels associated with the lower- and upper-manifolds, respectively. The

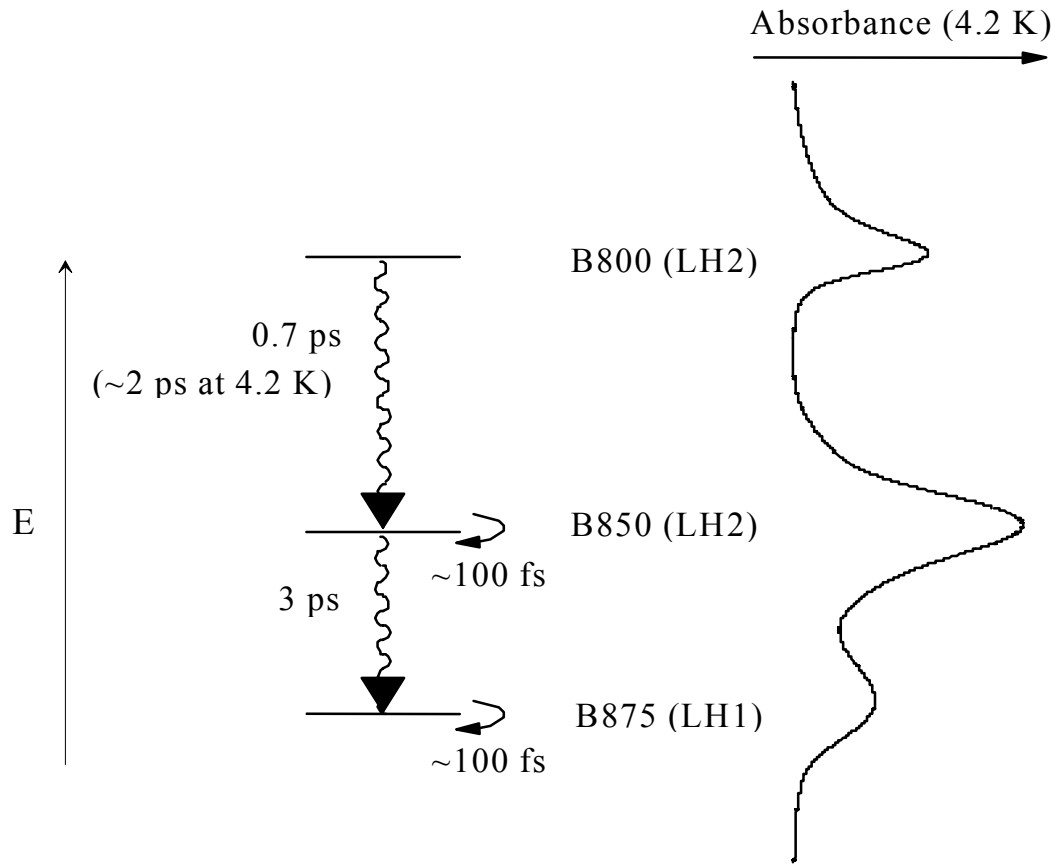

Figure 1.7 Low temperature (4.2 K) absorption spectrum of chromatophores from *Rps. acidophila* (strain 10050). At 4.2 K, the B800, B850 and B875 bands are located at ~ 804 nm, 870 nm and 905 nm, respectively. The B850 and B875 bands positions depend strongly on temperature [26], while the location of B800 band is almost temperature independent. The time constants of 0.7 and 3 ps apply respectively to the B800 ? B850 and B850 ? B875 energy transfer times at room temperature. The ~ 100 fs time constants correspond to inter-exciton level relaxations within the

(a)

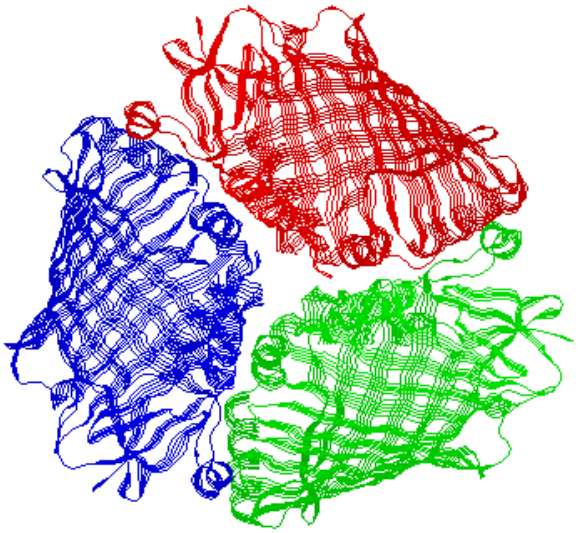

(b)

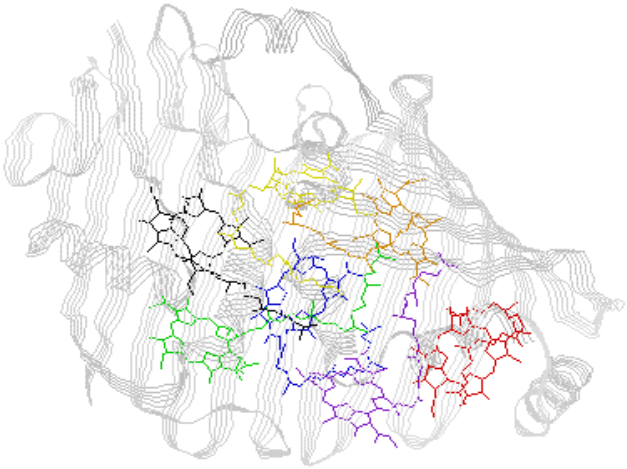

Figure 1.8 Part (a) shows arrangement of the FMO complex trimer from *Prosthecochloris aestuarii*, which has a three-fold symmetry. In Part (b), one subunit of the FMO complex showing seven BChls enclosed within an envelope of protein is described. The figures were generated by the program RasMol [15].

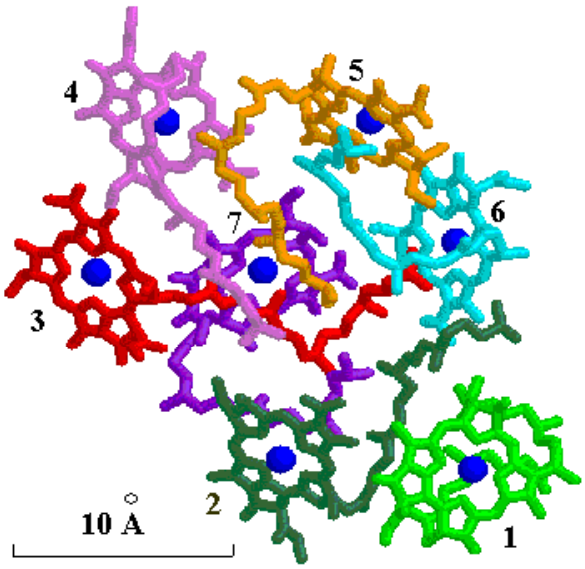

Figure 1.9 Arrangement of the 7 BChls in a subunit of FMO complex (trimer) from *Prosthecochloris aestuarii*. Blue dots shown in the center of BChls are Mg ions. The BChl numbering is given according to the scheme of Matthews and Fenna [54]. The nearest neighboring Mg–Mg distances are 11–15 Å and the phytyl chains are packed in the central space between the

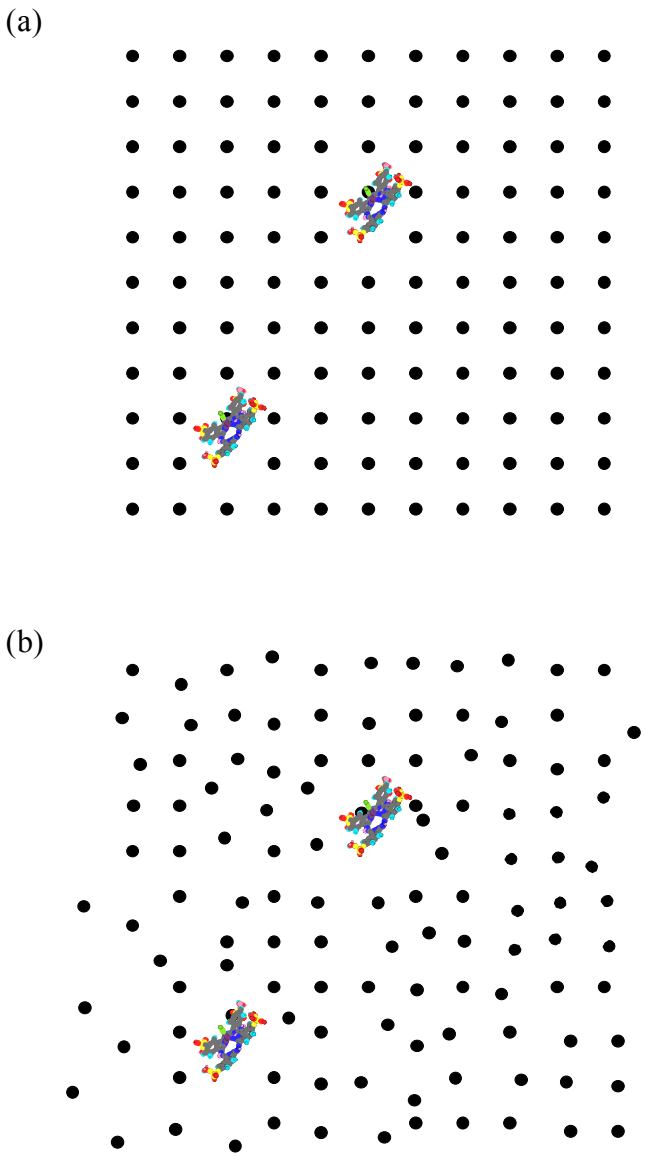

Figure 2.1 Parts (a) and (b) show schematic views of guest molecules in a perfect lattice (host) and in an amorphous lattice, respectively. In Part (a) the ZPLs appear at same transition frequency. However, in Part (b) the ZPLs appear at different frequencies, as shown in Figure 2.2.

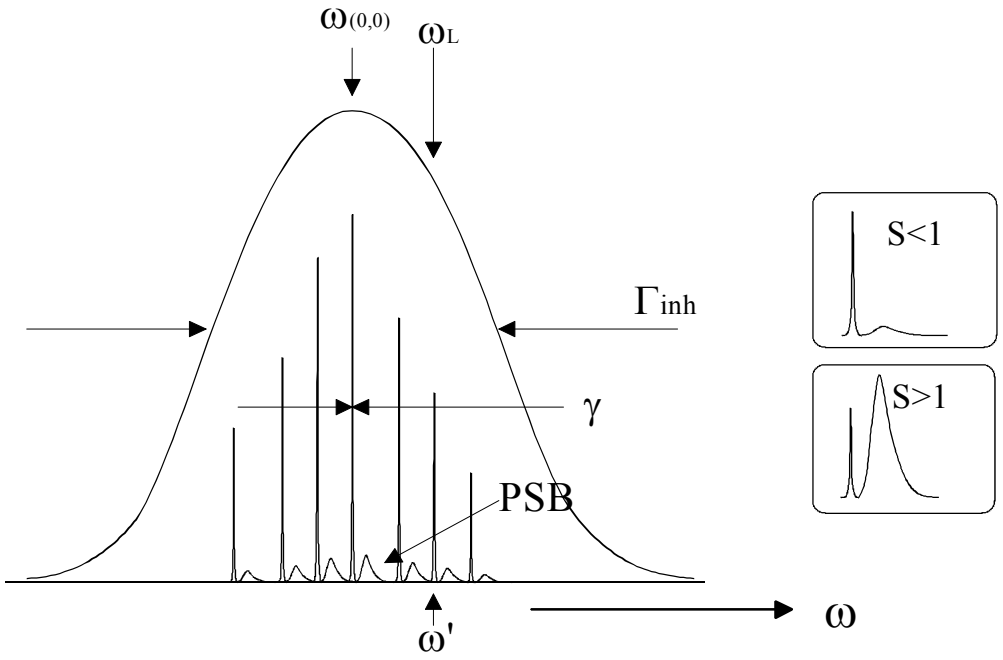

Figure 2.2 Diagram of homogeneously (γ) and inhomogeneously (Γ_{inh}) broadened absorption bands. The ZPLs and their phonon side bands are enlarged for clarification. ω_L is the laser frequency for selective excitation of a narrow isochromat. The windows at the right describe the schematic difference of the relative ZPL/PSB structures with respect to Huang-Rhys factor (electron-phonon coupling strength). Strong and weak coupling are defined by $S > 1$ and $S < 1$, respectively.

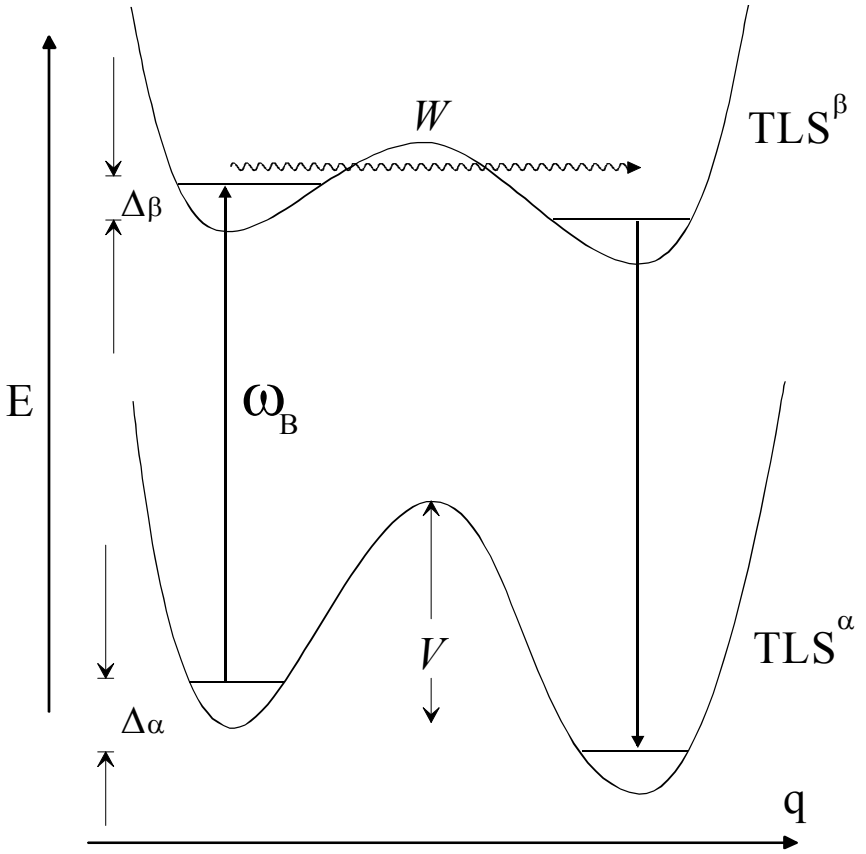

Figure 2.3 Diagram of TLSs coupled to a guest molecule in the ground state (α) and in the excited state (β). $\Delta\alpha$ and $\Delta\beta$ are asymmetry parameters and q represents the intermolecular coordinates. V is the amount of energy barrier and W ($=\omega_0\exp(-\lambda)$) is the tunneling frequency. ω_B stands for the excitation frequency. See text for details.

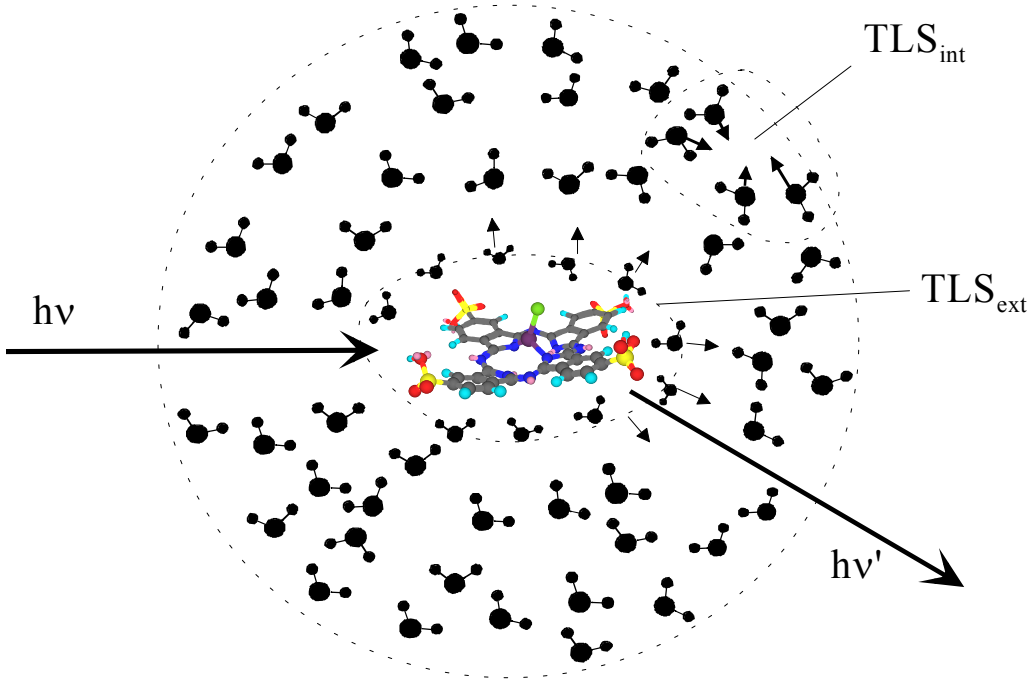

Figure 2.4 Schematic view of NPHB mechanism. See text for discussion. Original figure was prepared by Dr. Tonu Reinot (Dept. of Chem., Iowa State University).

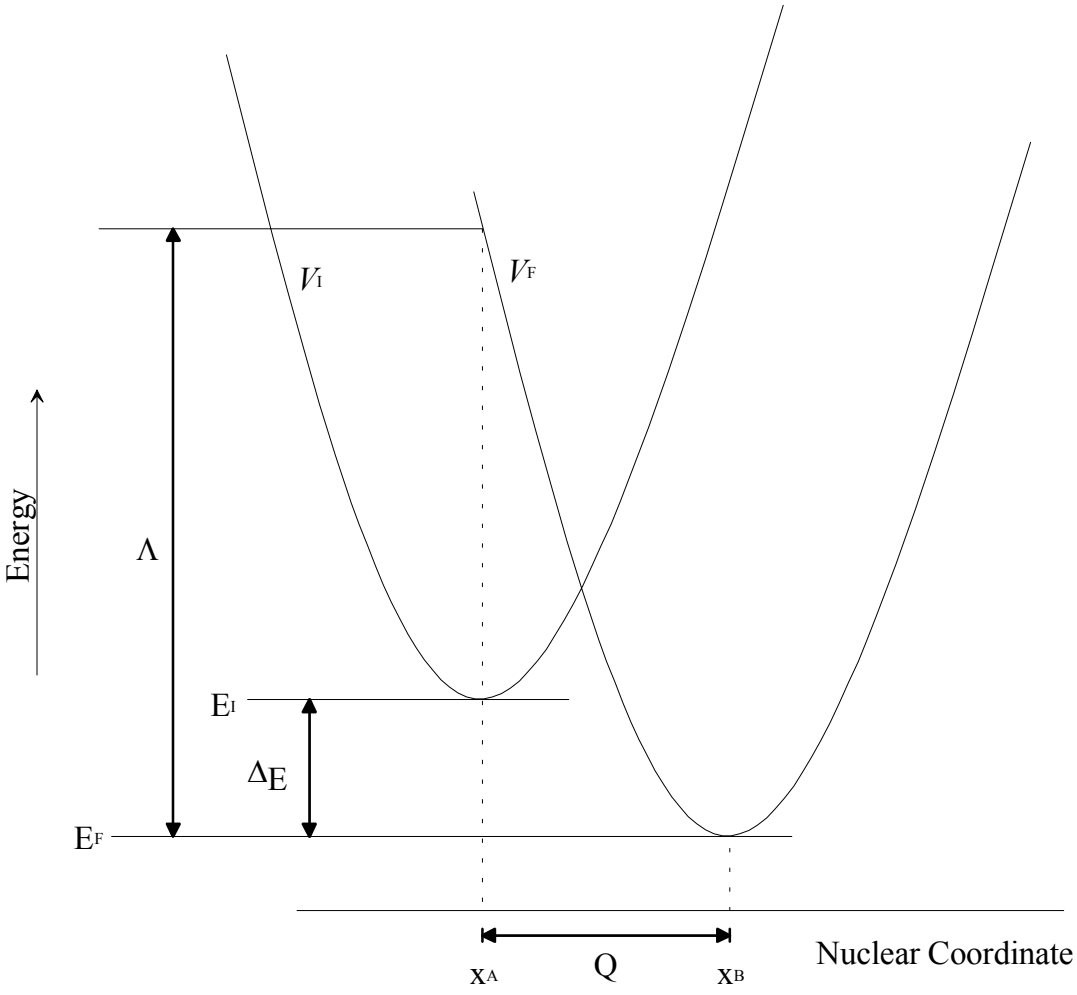

Figure 2.5 Scheme of the nuclear motions for a non-adiabatic energy transfer. Nuclear potential curves V_I and V_F correspond to donor and acceptor states, respectively. Note that the reorganization energy, Λ, is required to

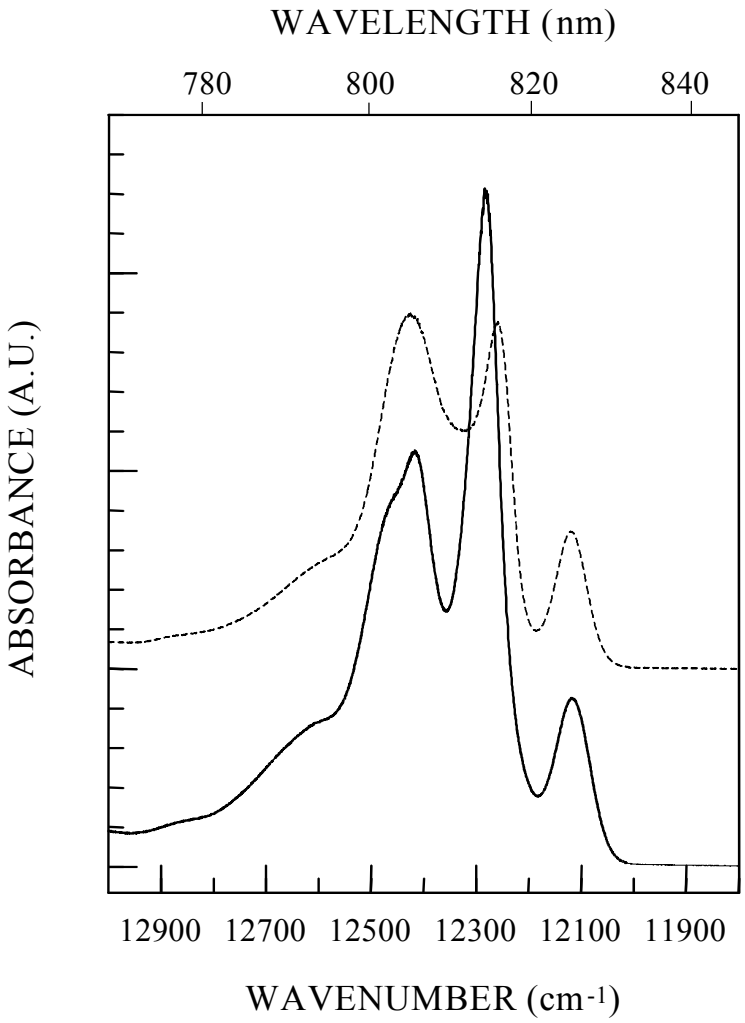
WAVELENGTH (nm)
780
800
820
840
ABSORBANCE (A.U.)
12900
12700
12500
12300
12100
11900
WAVENUMBER (cm-1)

Figure 1.

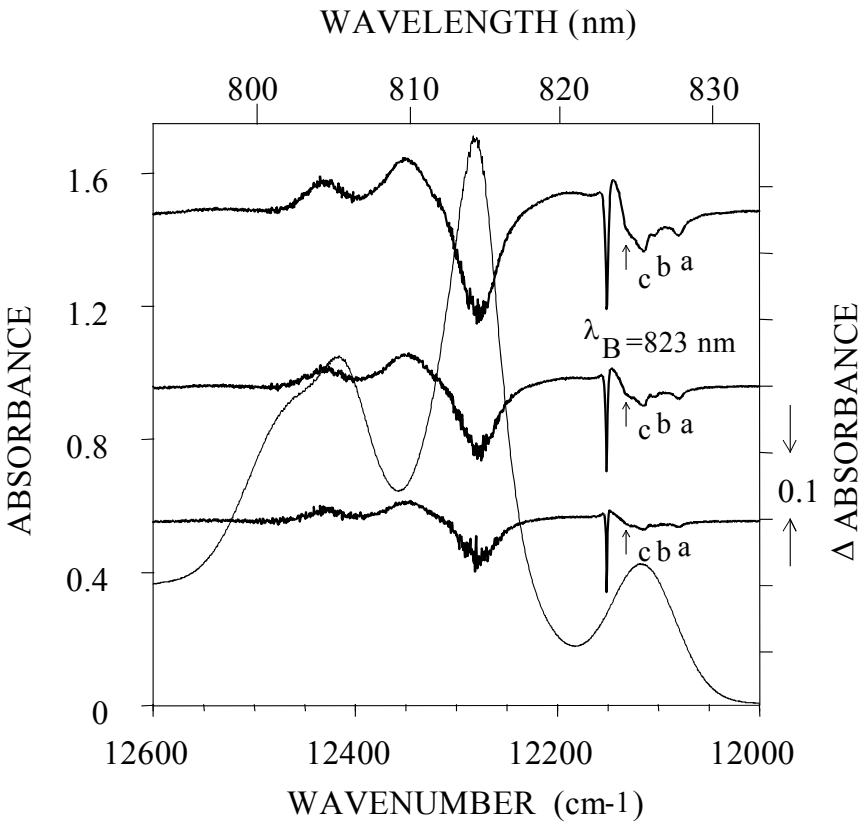
WAVELENGTH (nm)
800
810
820
830
1.6
1.2
0.8
0.4
0
ABSORBANCE
c b a
λB=823 nm
c b a
0.1
c b a
Δ ABSORBANCE
12600
12400
12200
12000
WAVENUMBER (cm-1)

Figure 2.

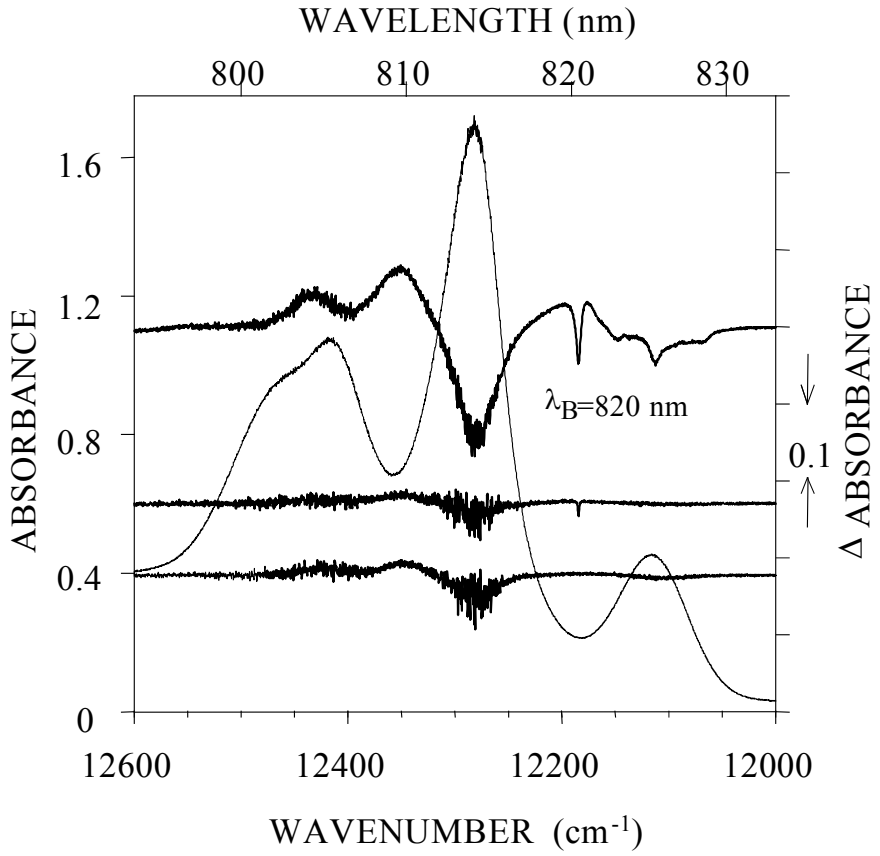
WAVELENGTH (nm)
800
810
820
830
1.6
1.2
0.8
0.4
0
ABSORBANCE
λB=820 nm
0.1
Δ ABSORBANCE
12600
12400
12200
12000
WAVENUMBER (cm-1)

Figure 3.

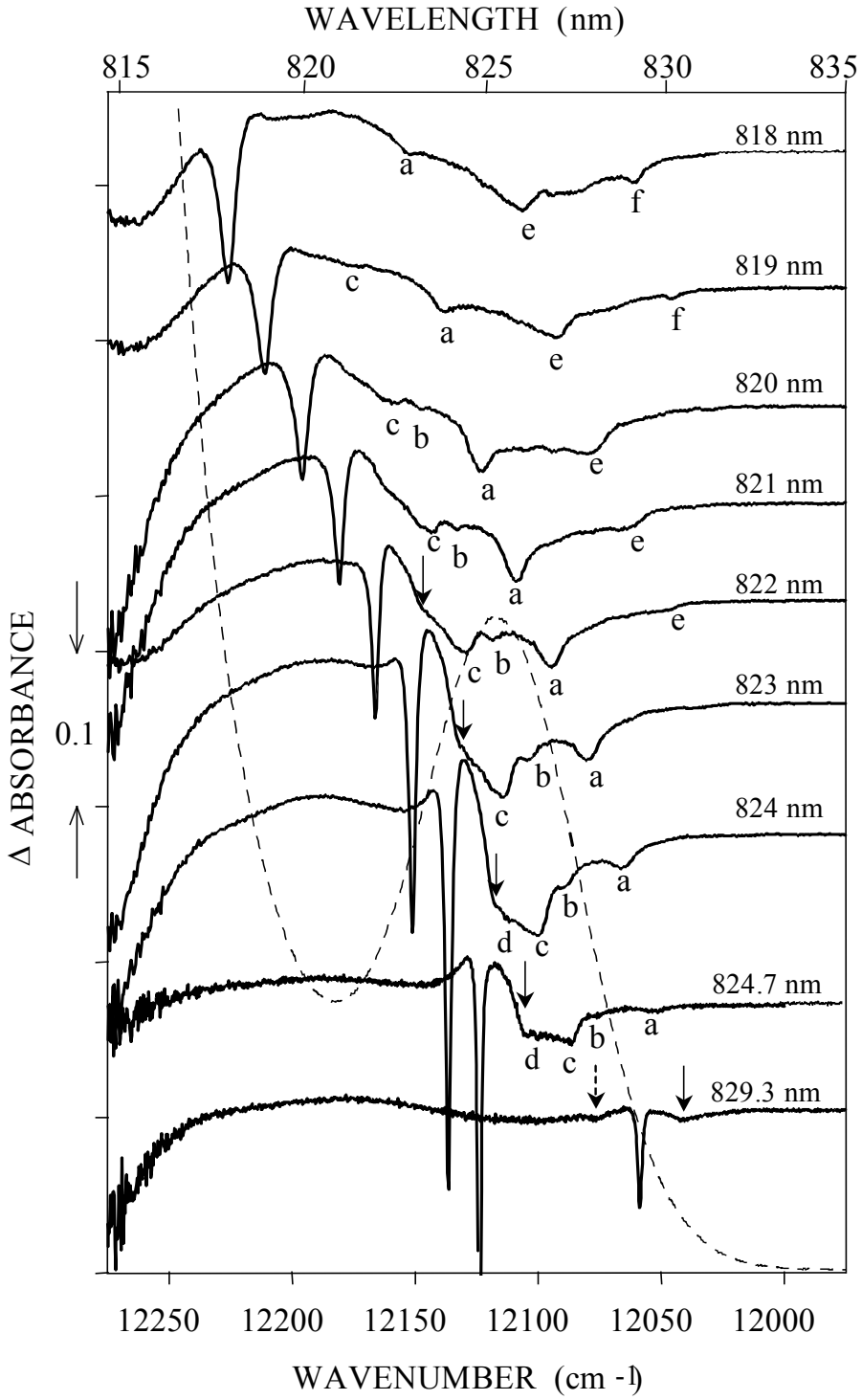
WAVELENGTH (nm)
815
820
825
830
835
818 nm
819 nm
820 nm
821 nm
822 nm
823 nm
824 nm
824.7 nm
829.3 nm
a
b
c
d
e
f
Δ ABSORBANCE
0.1
12250
12200
12150
12100
12050
12000
WAVENUMBER (cm -1)

Figure 4.

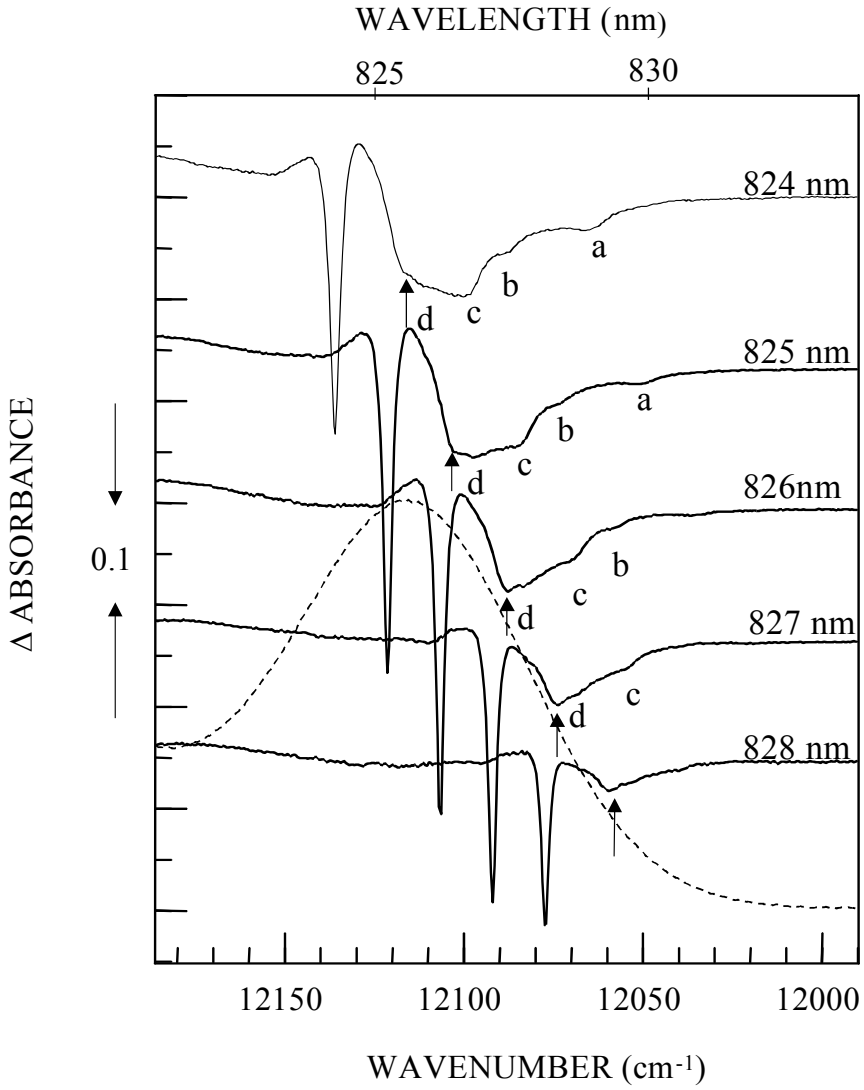
WAVELENGTH (nm)
825
830
824 nm
825 nm
826nm
827 nm
828 nm
a
b
c
d
Δ ABSORBANCE
0.1
12150
12100
12050
12000
WAVENUMBER (cm-1)

Figure 5.

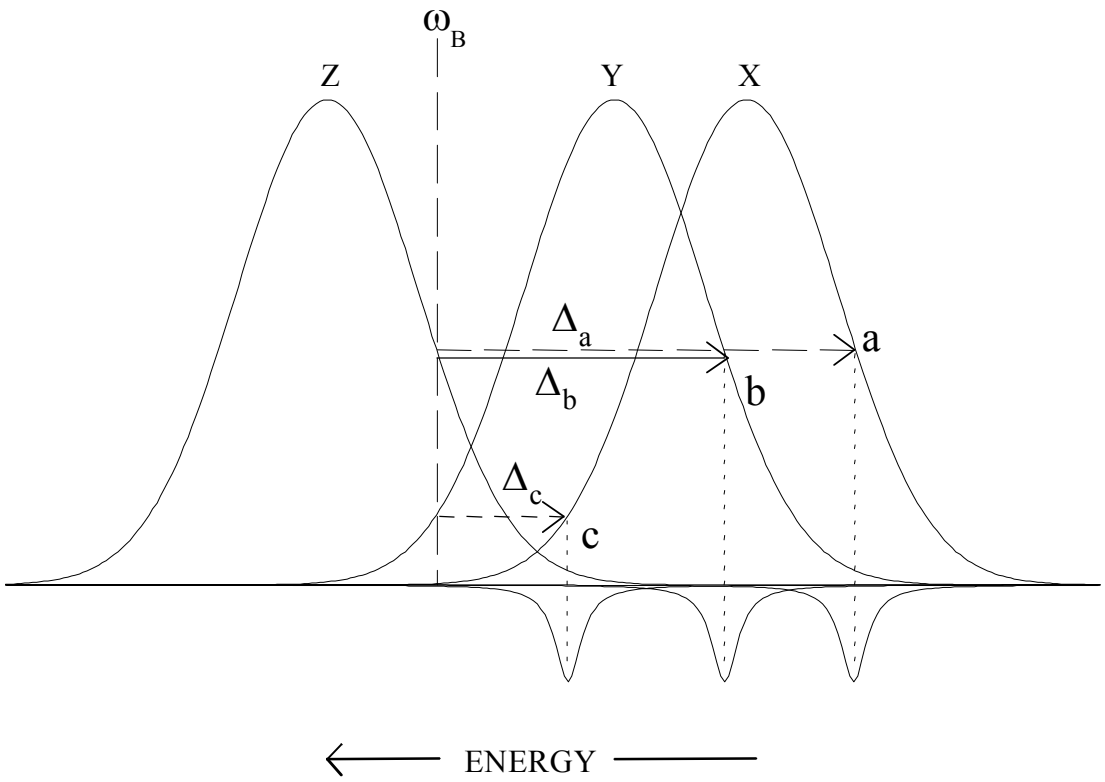

Figure 6.

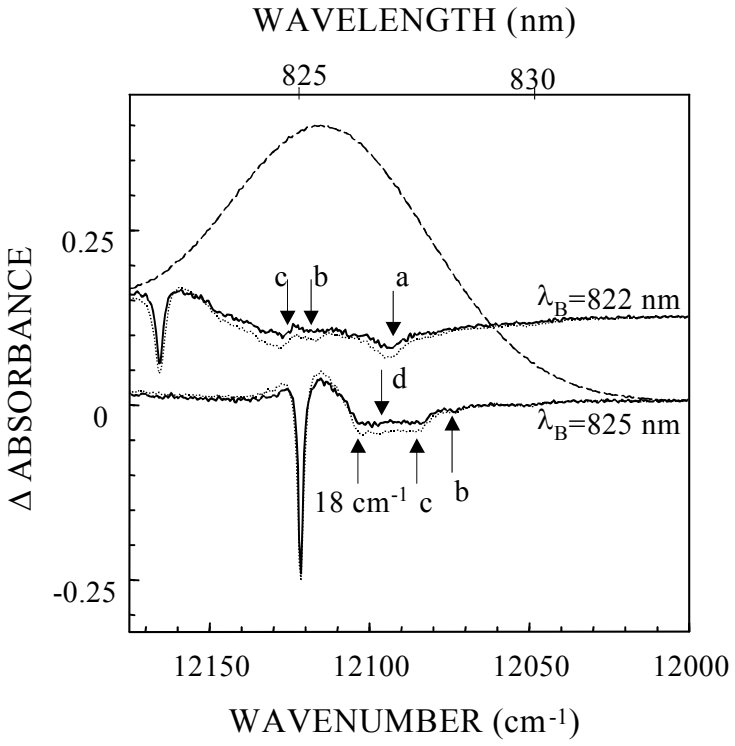
WAVELENGTH (nm)
825
830
0.25
0
-0.25
Δ ABSORBANCE
c
b
a
λB=822 nm
d
λB=825 nm
18 cm-1
c
b
12150
12100
12050
12000
WAVENUMBER (cm-1)

Figure 7.

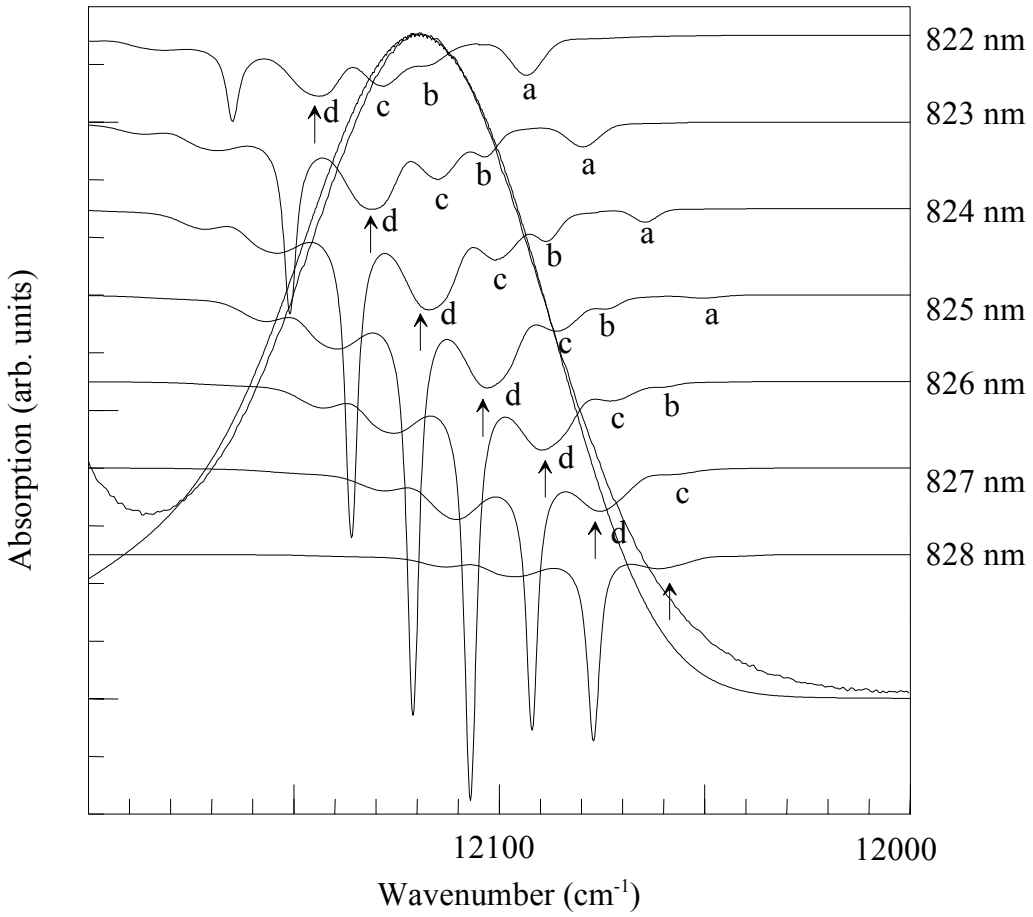
822 nm
823 nm
824 nm
825 nm
826 nm
827 nm
828 nm
a
b
c
d
Absorption (arb. units)
12100
12000
Wavenumber (cm-1)

Figure 8.

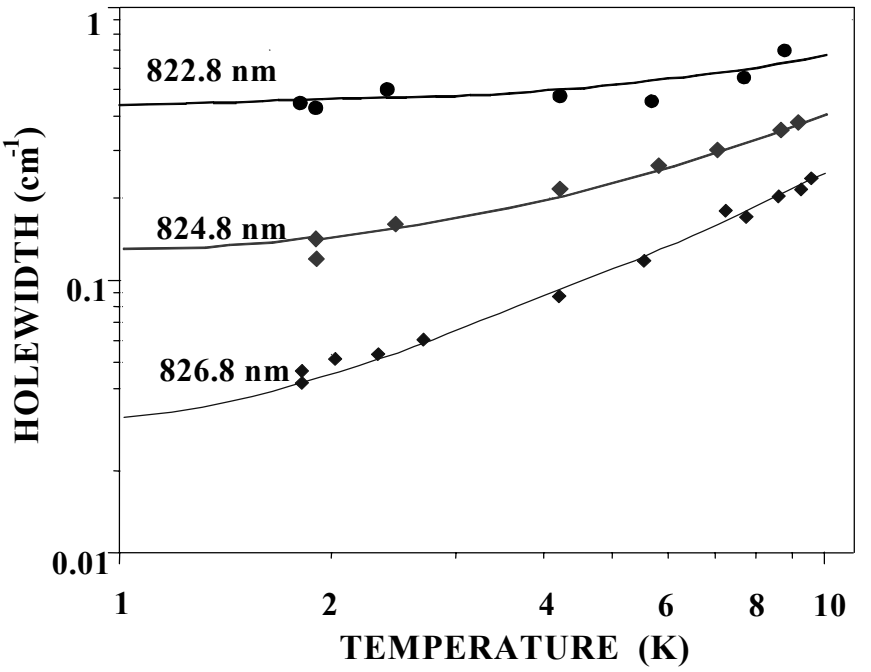
1
0.1
0.01
822.8 nm
824.8 nm
826.8 nm
HOLEWIDTH (cm-1)
1
2
4
6
8
10
TEMPERATURE (K)

Figure 9.

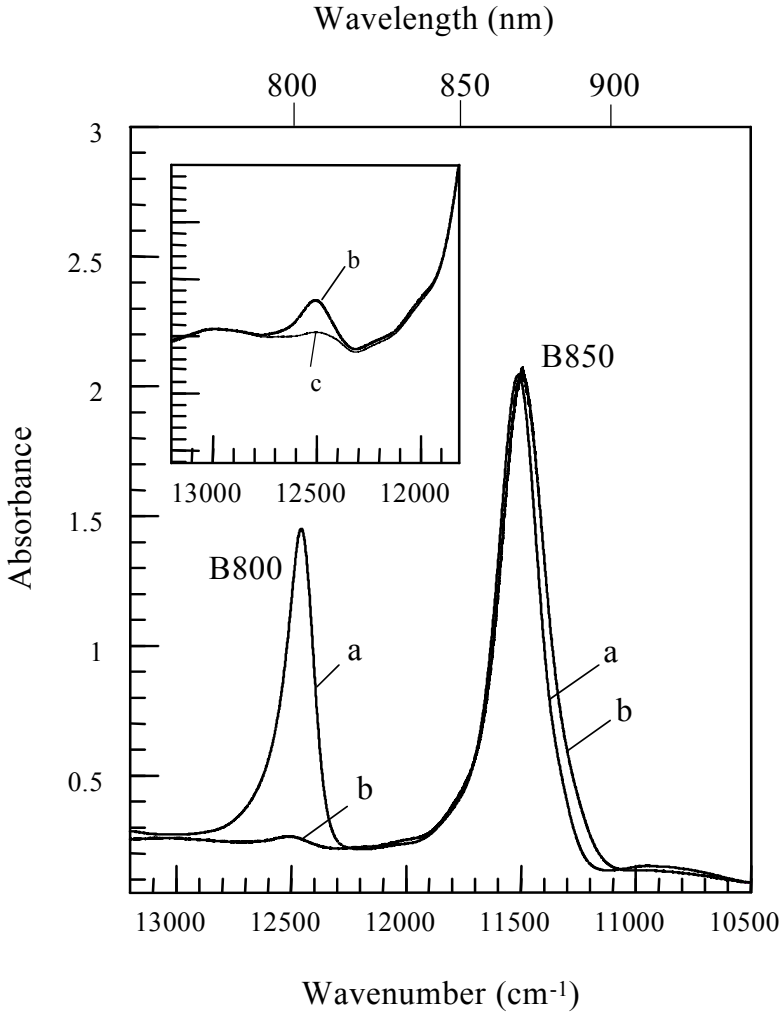
Wavelength (nm)
800
850
900
3
2.5
2
1.5
1
0.5
Absorbance
b
c
13000
12500
12000
B850
B800
a
a
b
b
13000
12500
12000
11500
11000
10500
Wavenumber (cm-1)

Figure 1.

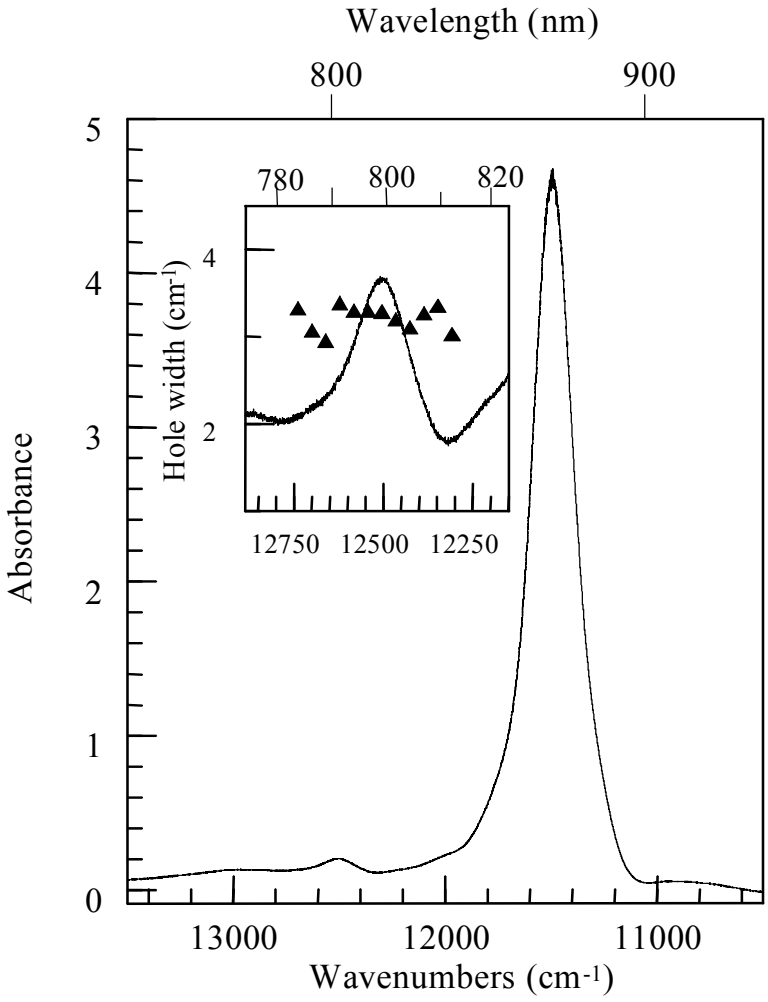
Wavelength (nm)
800
900
5
4
3
2
1
0
Absorbance
780
800
820
4
2
Hole width (cm-1)
12750
12500
12250
13000
12000
11000
Wavenumbers (cm-1)

Figure 2.

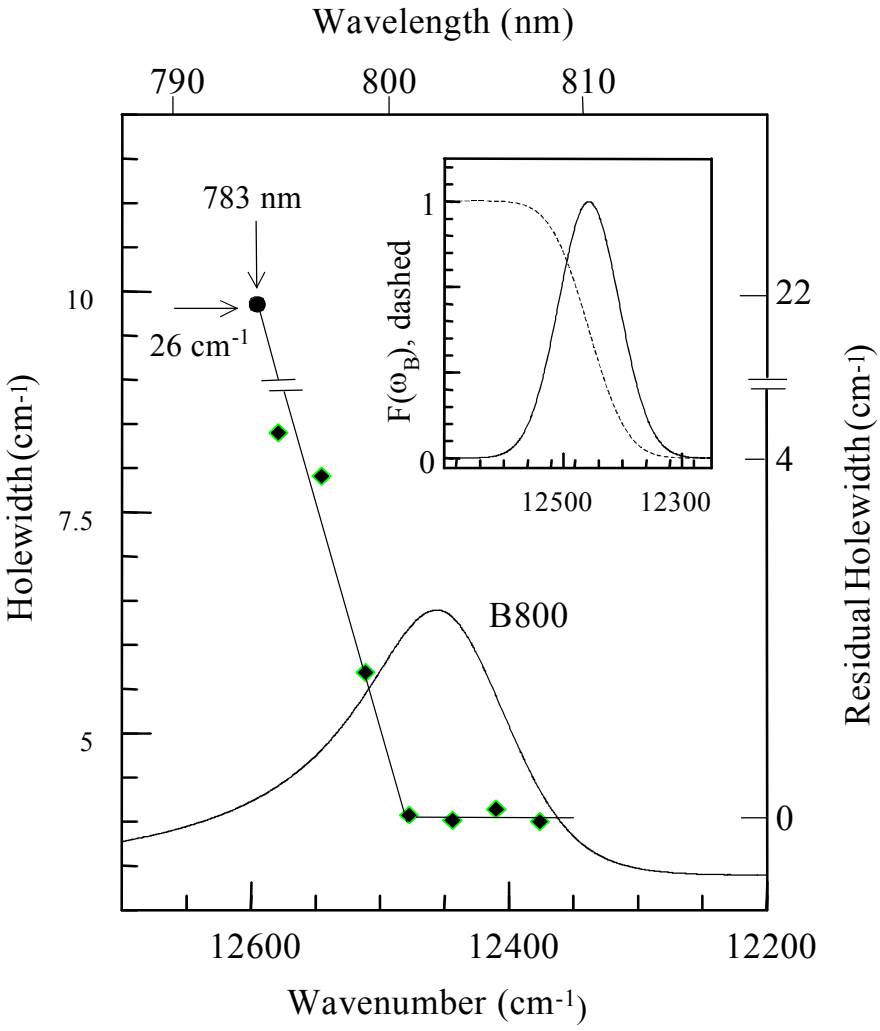
Wavelength (nm)
790
800
810
783 nm
26 cm-1
10
7.5
5
Holewidth (cm-1)
22
4
0
Residual Holewidth (cm-1)
B800
1
0
F(ωB), dashed
12500
12300
12600
12400
12200
Wavenumber (cm-1)

Figure 3.

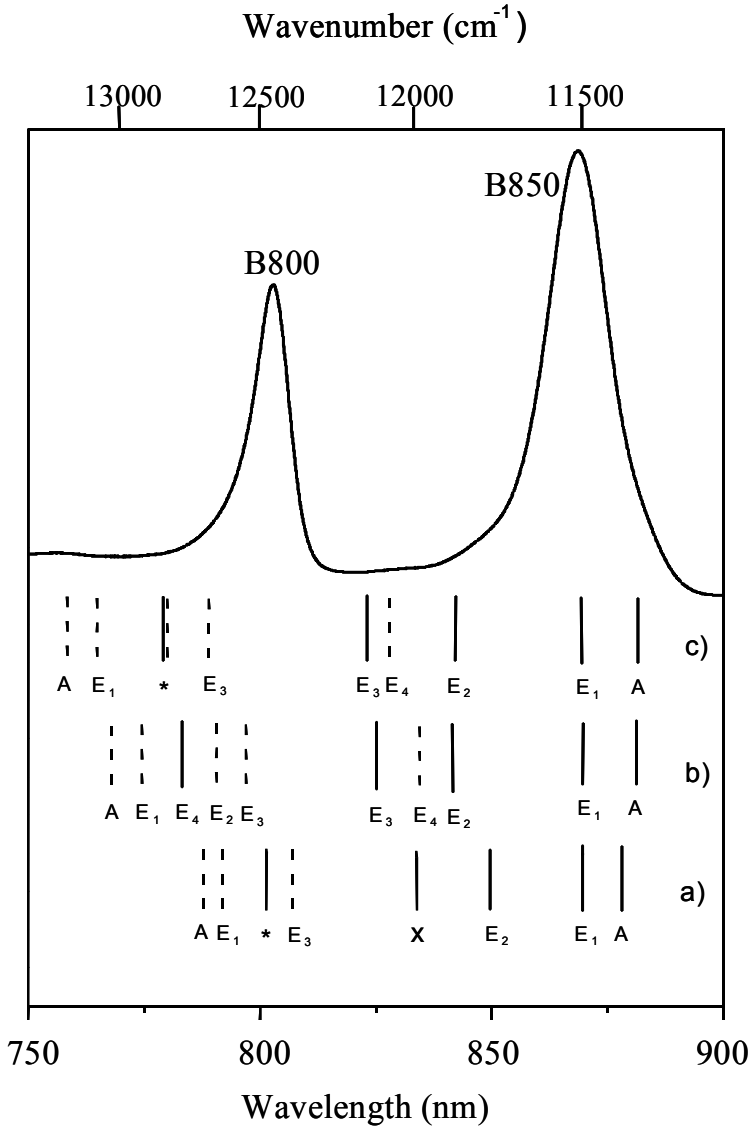
Wavenumber (cm-1)
13000
12500
12000
11500
B850
B800
A E1 * E3
E3 E4 E2
E1 A
c)
A E1 E4 E2 E3
E3 E4 E2
E1 A
b)
A E1 * E3
X
E2
E1 A
a)
750
800
850
900
Wavelength (nm)

Figure 4.

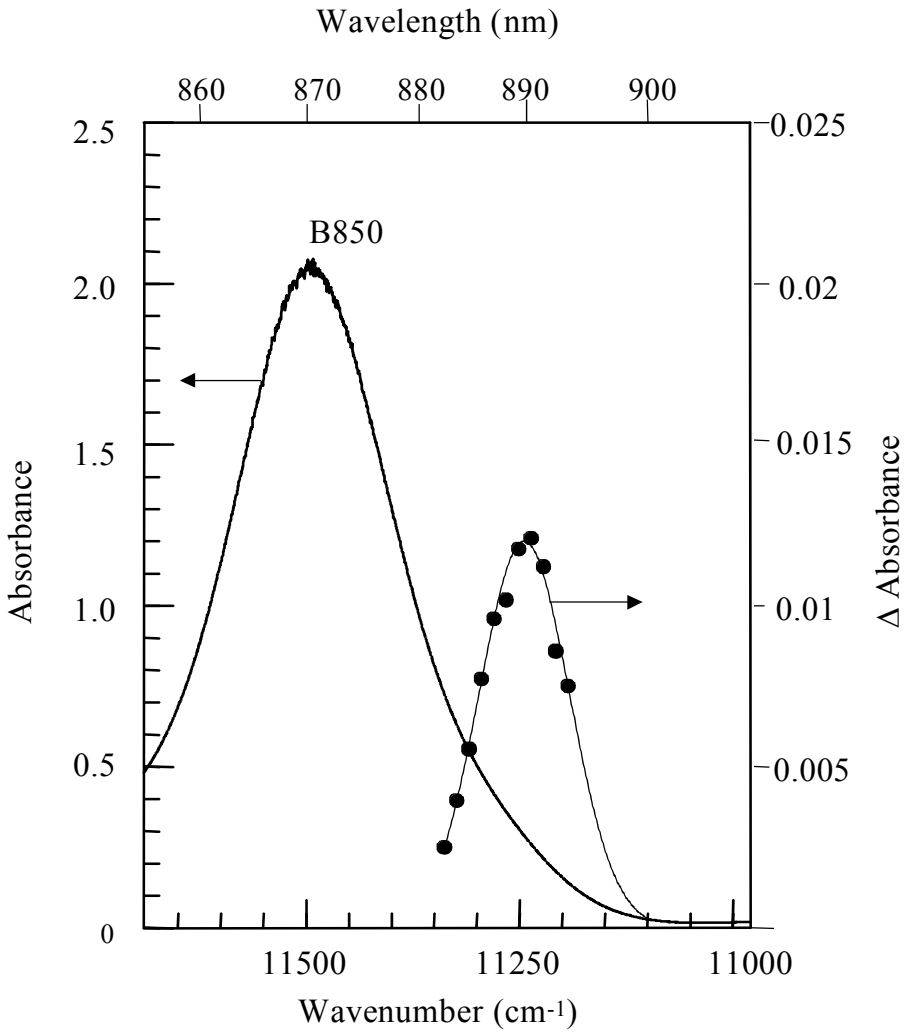
Wavelength (nm)
860
870
880
890
900
2.5
2.0
1.5
1.0
0.5
0
B850
Absorbance
0.025
0.02
0.015
0.01
0.005
Δ Absorbance
11500
11250
11000
Wavenumber (cm-1)

Figure 5.

Table 1.1 Simulated excitonic energies and dipole strengths for the FMO complexes

P. aestuarii[a]

State	State Energies, cm^{-1} (nm)	Dipole Strength, D^2	BChl
1	12111 (825.7)	49.7	3
2	12278 (814.5)	138.8	4
3	12312 (812.2)	60.6	1
4	12410 (805.8)	100.3	6
5	12488 (800.8)	71.1	7
6	12566 (796.4)	26.7	2
7	12610 (793.0)	34.6	5

C. tepidum[b]

State	State Energies, cm^{-1} (nm)	Dipole Strength, D^2	BChl
1	12113 (825.6)	48.9	3
2	12262 (815.5)	121.0	4
3	12355 (809.3)	79.5	1
4	12414 (805.6)	92.3	5,6
5	12448 (803.3)	59.8	7
6	12611 (793.0)	27.6	5,6
7	12649 (790.9)	52.2	2

[a]From simulation results described in Ref. [66].

[b]From Ref. [65].